SLAC-PUB-4822
December 1988
(A)

DISRUPTION, BEAMSTRAHLUNG, AND BEAMSTRAHLUNG PAIR CREATION*

PISIN CHEN
Stanford Linear Accelerator Center, Stanford, California 94309

SLAC-PUB--4822

DE89 007542

ABSTRACT

The two major effects from the interaction of e^-e^+ beams — beamstrahlung and disruption — are reviewed, with emphasis on flat beam collisions. For the disruption effects we discuss the luminosity enhancement factor, the maximum and *rms* disruption angles, and the "kink instability". All the results are obtained from computer simulations, and scaling laws based on these are deduced whenever possible. For the beamstrahlung effects, we concentrate only on the final electron energy spectrum and the deflection angle associated with low energy particles. In addition to the generic studies on the beam-beam effects, we also list the relevant beam-beam parameters obtained from simulations on two sample designs: the TLC and the ILC. As an addendum, the newly discovered phenomenon of coherent beamstrahlung pair creation, together with the incoherent process, are discussed.

INTRODUCTION

There are two major phenomena induced by the beam-beam interaction which are important to the design of high energy linear colliders. Namely, the *disruption* process where particle trajectories are bent by the field provided by the oncoming beam, and the *beamstrahlung* process where particles radiate due to the bending of the trajectories. The most important impact of disruption is the deformation of the effective beam sizes during collision, which causes an enhancement on the luminosity. In addition, the disruption angle affects the constraints on the final quadrupole aperture. When the two beams are colliding with certain initial offset, the disruption effect between the two beams would induce a kink instability, which imposes a constraint on beam stability. Ironically, this instability helps to relax the offset tolerance for flat beams, because the offset beams tend to find each other during the initial stage of the instability. Under a multi-bunch collision mode, however, the kink instability will largely degrade the luminosity through the relatively long growth time. On the other hand, the direct impact of beamstrahlung is the loss of the available energy for high energy events, and the degradation of beam energy resolution because of the stochastic nature of the radiation.

Most of the issues raised above can be studied by decoupling the disruption and the beamstrahlung effects. The energy loss due to beamstrahlung may modify the luminosity enhancement but this effect can be ignored since we are only interested in the case where the average energy loss is small. Conversely, the average energy loss and the final energy spectrum can be studied by assuming no disruption without compromising too much on accuracy. There is, however, one issue where the two effects are strongly coupled. This is the maximum disruption angle associated with the large deflections from particles that have suffered severe energy loss.

In this report we summarize what has been studied on these issues with emphasis on flat beam collisions. The computer simulations are performed using the code ABEL (Analysis of Beam-beam Effects in Linear colliders) described in Ref. 1, but improved considerably since it was first written. Some results given here are still preliminary and will be refined in later papers, but their qualitative features will not be changed.

LUMINOSITY ENHANCEMENT

Our primary interest is the enhancement of luminosity due to the mutual pinching of the two colliding beams. The details have been discussed in Ref. 2 for round beams and will be given in Ref. 3 for flat beams. As was pointed out in Ref. 2, the luminosity is infinite if the initial beam is paraxial and the computation is perfectly accurate. This is because a paraxial beam can be focused to a singular point. In reality, however, a beam will always have certain inherent divergence, and the singularity is only approached asymptotically. To account for this effect, a parameter $A_{x,y} = \sigma_z/\beta^*_{x,y}$ is introduced,[2] which is proportional to the emittance for a given beam size $\sigma_{x,y}$. The computed enhancement factor $H_D = L/L_0$, where L_0 is the geometrical luminosity without the effect of the depth of focus related to $A_{x,y}$ taken into account, is plotted in Fig. 1 as a function of D_y and A_y for flat beams.

The data in Fig. 1 are obtained by using a distribution function which is uniform in x and Gaussian in y and z (UGG), instead of a three-dimensional Gaussian distribution (GGG), for easiness of computation. The enhancement factor of GGG distributions for a given D_y can be

* Work supported by the Department of Energy, contract number DE-AC03-76SF00515.

Contributed paper at the DPF Summer Study Snowmass '88, High Energy Physics in the 1990's, Snowmass, Colorado, June 27-July 15, 1988

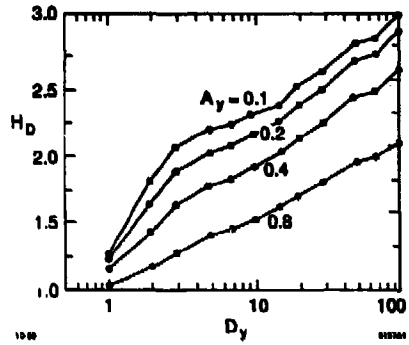

Fig. 1. Luminosity enhancement factor for flat beams.

deduced from a superposition of UGG results with disruption parameters ranging from 0 near the horizontal edge to $\sqrt{6/\pi}D_y$ at the beam center. The enhancement factor for round beams is shown in Fig. 2.

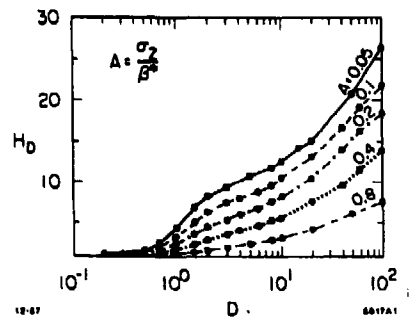

Fig. 2. Luminosity enhancement factor, round beams.

By comparing Figs. 1 and 2, one finds that the enhancement factor for flat beams scales roughly as the cube-root of the corresponding value for round beams; which obeys the following empirical scaling law that fits all data points in Fig. 2 to within 10% accuracy:

$$H_D = 1 + D^{1/4}\left(\frac{D^3}{1+D^3}\right)\left[\ln(\sqrt{D}+1) + 2\ln\left(\frac{0.8}{A}\right)\right] \quad . \quad (1)$$

The reason for the flat beam enhancement not being scaled as a square root of the corresponding value for the round beam is because the horizontal focusing can enhance the vertical pinch effect (and vice versa) in the round beam case, whereas for flat beams the pinch in the major (horizontal) dimension can hardly affect the disruption in the minor dimension.

In both cases, our results indicate a logrithmic divergence of H_D as a function of A, or A_y. In addition, H_D is monotonically increasing as a function of D, or D_y, at least up to D =100. This second finding of ours is qualitatively the same as that found by Fawley and Lee[4] but in contradiction to Holebeek[5] and Solyak;[6] where the enhancement factor first saturates before eventually decreases at large D's.

The difference appears to be due to the different ways of handling stochastic errors. In a Monte Carlo simulation such as ours, the initial condition is generated by random numbers, which introduces a statistical fluctuation, and therefore an asymmetry, of the order $1/\sqrt{N_p}$, N_p being the number of macro particles. This asymmetry will be amplified during collision (i.e., kink instability) due to the beam-beam force, especially when the disruption parameter is large. The fact that the number of macro particle in a simulation is typically much smaller than the actual particle number, this fluctuation is artificially enhanced if no proper action is taken. To minimize this computation error, the particle distribution function is symmetrized at every time step in our calculation, so that the beam-beam force has the up-down symmetry at all times for the flat beam case. Similarly, in the round beam case only the radial force is computed. This process eliminates the possible instability triggered by computation errors.

The actual collisions are expected to have some unavoidable initial offset in alignment and skewness in distributions. Since the asymmetry in distributions tend to shift the center-of-gravity of the beams, it gives rise to the same effect as the initial alignment offsets. For this reason our study on the effect of imperfections is concentrated on initial offsets only.

As will be discussed in the next section, an initial offset triggers a kink instability, especially when the disruption parameter becomes large. As it occurs, this instability is not always harmful because, in the initial phase of the instability, the beams always tend to find each other, which prevents the otherwise rapid degradation of the luminosity for large initial offsets. Figure 3 shows the luminosity enhancement factor as a function of offset Δ_y (in units of σ_y) for various values of D_y. The dotted curve is the geometrical enhancement factor without beam-beam force, which is equal to $\exp(-\Delta_y^2/4)$. UGG distribution is used and A_y =0.2 for all curves. The up-down symmetry is not enforced except for the cases at Δ_y =0.

From Fig. 3 one finds that the tolerance on alignment offset reaches an optimum for values of D_y between 5 and 10. Within this range of D_y, H_D is still above unity even at $\Delta_y \sim 3$. Beyond this region of D_y the beam-breakup becomes severe while below which the beam-beam attraction is not yet strong enough.

The same data as in Fig. 3 is replotted in Fig. 4 as a function of D_y and each curve corresponds to a fixed value of Δ_y. (The region of large D_y and small Δ_y is not very accurate because of its sensitivity to computing errors.) One sees a saturation and decrease of H_D as a function of D_y unless $\Delta_y = 0$. One also notices that the curves with small offsets, e.g., $\Delta_y = 0.2$, resemble the results in Refs. 5 and 6, except that our offset was explicitly

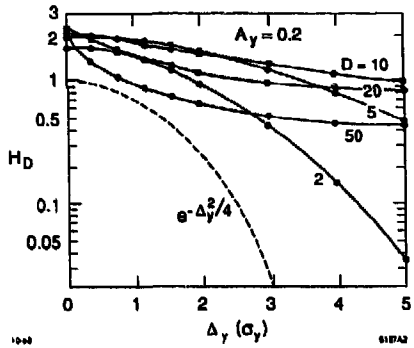

Fig. 3. H_D as a function of offset; Flat beams.

introduced. In designing a linear collider, one needs to estimate H_D for the chosen D and A. This depends on the assesment of potential imperfections of beam-beam collision. Though arbitrary, it may be safer to adopt the curve for $\Delta_y = 0.2$ or 0.4, instead of $\Delta_y = 0$, as the effective enhancement factor.

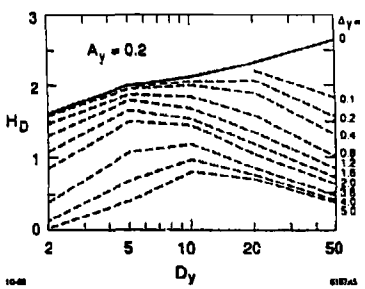

Fig. 4. H_D as a function of D_y; Flat beams.

Similar exercise for round beams are shown in Fig. 5 for D up to 50. Here we find the generic behavior as in the case for flat beams.

DISRUPTION ANGLE

Information on the final direction of the electron trajectory after collision is necessary in designing the interaction region, especially for the aperture of the final quadrupole magnets. If the disruption parameter is very small, the transverse location of a particle during collision is nearly constant. Then we can estimate the disruption angle θ_x

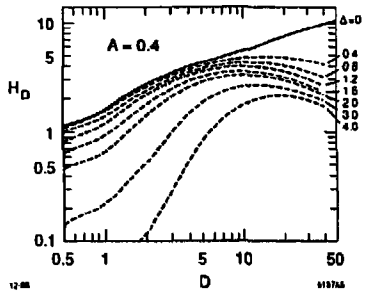

Fig. 5. H_D as a function of offset; Round beams.

and θ_y as functions of the initial transverse coordinates x_0 and y_0. For very flat Gaussian beams we have

$$\theta_x = -\sqrt{\frac{\pi}{2}} D_x \frac{\sigma_x}{\sigma_z} \mathcal{I}m\left[\frac{i}{\pi}\int_{-\infty}^{+\infty} \frac{\exp(-t^2)dt}{(x_0/\sqrt{2}\sigma_x) - t - i0}\right] \quad , \quad (2)$$

$$\theta_y = -\sqrt{\frac{\pi}{2}} D_y \frac{\sigma_y}{\sigma_x}\left[\frac{2}{\sqrt{\pi}}\int_0^{y_0/\sqrt{2}\sigma_y} e^{-t^2}dt\right] e^{-x_0^2/2\sigma_x^2} \quad , \quad (3)$$

where the quantities in the square brackets can be expressed by the complex error function $w(x_0/\sqrt{2}\sigma_x)$ and the real error function $\mathrm{erf}(y_0/\sqrt{2}\sigma_y)$. Here the emittance is ignored. One finds that the maximum and *r.m.s.* disruption angles to be

$$\theta_{x,max} = 0.765 D_x \frac{\sigma_x}{\sigma_z} \quad , \quad (x_0 = 1.31\sigma_x) \quad (4)$$

$$\theta_{y,max} = \sqrt{\pi/2} D_y \frac{\sigma_y}{\sigma_z} \quad , \quad (x_0 = 0,\ y_0 = \infty) \quad (5)$$

$$\theta_{x,rms} = \sqrt{\pi/(6\sqrt{3})} D_x \frac{\sigma_x}{\sigma_z} \quad ,$$

$$\theta_{y,rms} = \sqrt{\pi/(6\sqrt{3})} D_y \frac{\sigma_y}{\sigma_z} \quad . \quad (6)$$

(Rigorously speaking, for flat beams with large but finite aspect ratio, θ_y reaches a maximum near $y_0 \sim \sigma_x$ and then decreases; but this is not important.)

The distribution functions of θ_x and θ_y are shown in Fig. 6. The actual singularities at $\theta_x = \theta_{x,max}$ and $\theta_y = 0$ are not supposed to be as sharp as those in Fig. 6 because of finite emittance, various errors, and the disruption effect. However, we found from simulations that the qualitative difference between the horizontal and vertical angles still holds even for $D_{x,y}$ not much less than unity.

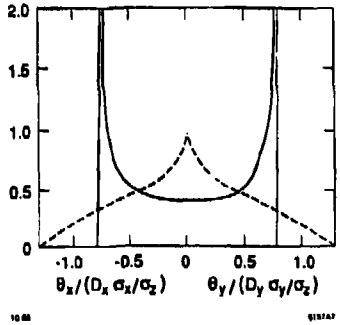

Fig. 6. Distribution of $\theta_{x,y}$ for small $D_{x,y}$.

Figure 7 shows the maximum and r.m.s. vertical disruption angle, in units of $D_y\sigma_y/\sigma_z$, as a function of D_y. Here we consider the case for small D_x only. The four curves corrrspond to A_y = 0.1, 0.2, 0.4, 0.8, respectively. The dependence on A_y is not as significant as in the case of H_D except for the small D_y region, where the beam divergence is emittance dominated. (The distribution of initial σ_z is truncated at 2.5 standard deviations in the simulation.)

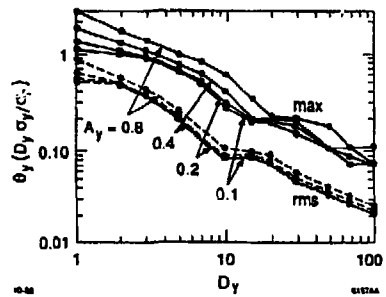

Fig. 7. Maximum and r.m.s. vertical disruption angle.

The simulation results can roughly be fitted by

$$\theta_{y,rms} \sim \sqrt{\frac{\pi}{6\sqrt{3}}}\frac{\sigma_y}{\sigma_z}\frac{D_y}{[1+(0.5D_y)^5]^{1/6}} \qquad (7)$$

and $\theta_{y,max} \sim 2.5\theta_{y,rms}$. Here the contribution of the initial emittance ($= A_y\sigma_y/\sigma_z$ for $\theta_{y,rms}$) has not been included. The reason that the angle does not increase linearly in D_y is that the particle trajectories are bent backwards and oscillate when D_y is large.

So far, the collision is assumed to be head-on. For flat beams the disruption angle in the presense of vertical offset is also important in determining the aperture of the final quads. The mean deflection angle of the entire bunch can be written in the form[7]

$$\Theta_y = \frac{1}{2}\frac{\sigma_y}{\sigma_z}D_y H_c(D_y,\Delta_y) \quad . \qquad (8)$$

where Δ_y is the vertical offset in units of σ_y and the weak dependence on A_y is ignored. For small disruptions, the function H_c approaches the following analytic form

$$H_c(D_y,\Delta_y) = \int_0^{\Delta_y} e^{-y^3/4}dy \quad . \qquad (9)$$

Figure 8 shows H_c as a function of Δ_y computed by simulations, where UGG distribution is assumed.

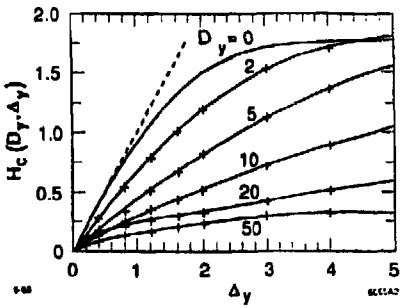

Fig. 8. Effective center-of-mass deflection.

Roughly speaking, the maximum disruption angle in the presense of offsets is the sum of the center-of-mass deflection angle Θ_y and the maximum angle in the absense of offsets, $\theta_{y,max}$.

KINK INSTABILITY

If one of the beams is displaced vertically for some reason, this offset triggers a vertical oscillation and, when D is large, the oscillation is enhanced by the beam-beam force. This phenomena is known as the *kink instability*. Figure 9 shows a specific example.

In the above figure the bunch is sliced longitudinally and the vertical coordinate y of the center-of-mass of each slice (in units of σ_y) is plotted against the longitudinal coordinate s (in units of σ_z). Each graph corresponds to a snapshot of the beam vertical position at a particular time t (in units of σ_z/c). The development of the instability can be seen in time sequence. The initial offset in this example is chosen to be $0.2\sigma_y$ (full) and the disruption parameter is $D_y = 20$.

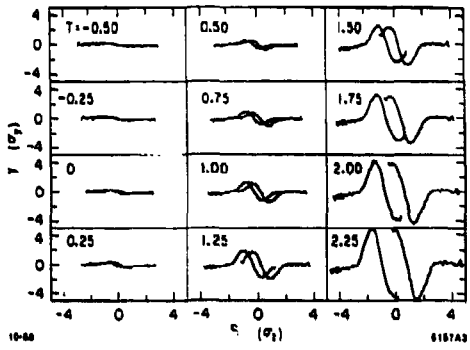

Fig. 9. An example of kink instability.

e⁻ and e⁺ beams is varified to be $\pi/3$, and the growth rate is as predicted. Furthermore, Fig. 9 clearly demonstrates the standing-wave nature of the kink instability, which agrees with the description of Eq. (11).

So far our discussion on the kink instability deals with collisions of two bunches. Another type of kink instability occurs during the collision of two bunch trains, each consists of N_B bunches. One of the major problems of such a multibunch operation is the interactions between bunches before and after their collisions at the central collision point. The i^{th} bunch in the electron bunch train will collide not only with the i^{th} bunch in the positron train, but also with the $j(<i)^{th}$ positron bunch before its coming to the central collision point. Colliding two flat beams at a relatively large crossing angle can help to avoid unwanted direct encounters between the outgoing bunch debris and the incoming fresh bunches. However, due to the long-

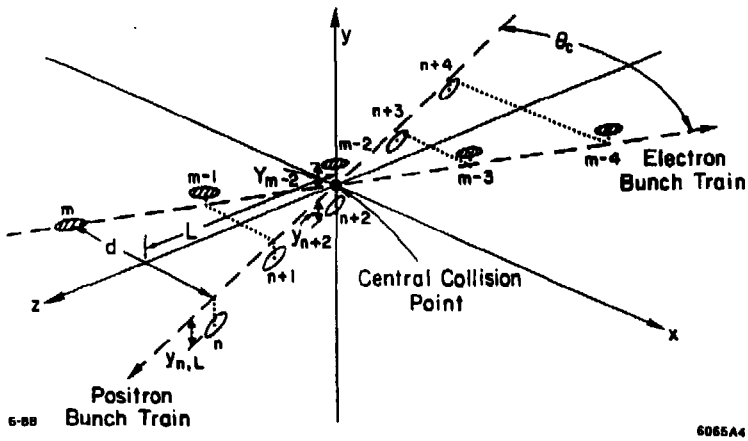

Fig. 10. Schematic diagram for collisions of bunch trains.

For uniform beams and small amplitude oscillations, the equation of motion for the beam particles can be obtained from fluid dynamics (the flat beam version of the equation is given in Ref. 8),

$$\left[\frac{\partial}{\partial t} \pm \frac{\partial}{\partial s}\right]^2 y_\pm = -\omega_0^2 (y_\pm - y_\mp), \quad \omega_0^2 = \frac{\sqrt{2\pi}}{6}\frac{D_y}{\sigma_z^2} \quad , \quad (10)$$

where $y_\pm$ is the y coordinate of $e^+$and e^- beams. The most unstable solution is found to be

$$y_\pm = \text{const.} \times \exp\left[\pm i\left(\frac{\sqrt{3}}{2}\omega_0 s - \frac{\pi}{6}\right) + \frac{1}{2}\omega_0 t\right] \quad . \quad (11)$$

This solution is in reasonable agreement with the simulation shown in Fig. 9. Namely, the phase difference between

range nature of the Coulomb interaction, there still exists undesirable interference between two separated bunches at a distance. Since the crossing angle cannot be made arbitrarily large due to the luminosity consideration, this long range interaction cannot be entirely suppressed. In fact, it imposes a severe restriction on the stability of the beams.

Consider the encounter between the n^{th} positron bunch after collision and the m^{th} $(m > n)$ electron bunch before collision at a distance L from the collision point. A schematic diagram of the system is shown in Fig. 10. We assume that all the bunch encounters occur within the drift space around the central collision point.

According to Eq. (8), the center-of-mass deflection angle for the n^{th} positron bunch is

$$\Theta_{yn} = \frac{1}{2}\frac{\sigma_y}{\sigma_z} D_y H_c(D_y, \Delta_{yn}) \quad , \quad (12)$$

where Δ_{yn} is the relative offset between the m^{th} electron and the n^{th} positron bunch, in units of σ_y, at their closest encounter. The cumulative offset for the m^{th} bunch before arriving at the central collision point is therefore

$$\Delta_m = C \sum_{n<m} H_c(D_y, \Delta_n) + \delta_m \quad , \qquad (13)$$

where δ_m is the initial offset of the m^{th} beam, and the coefficient C is

$$C = D_x D_y \left(\frac{\theta_d}{\theta_c}\right)^2 \quad , \qquad (14)$$

and $\theta_d = \sigma_x/\sigma_z$ is the diagonal angle of the bunch.

The cumulative offset Δ_m (in units of $\delta(1+C)^{m-1}$) is plotted as a function of the number of bunches in Fig. 11. Since the factor θ_d/θ_c must be larger than unity in order that the crossing angle does not reduce the luminosity significantly, the condition for negligible growth of the instability, i.e., $\Delta_{yn} \lesssim \delta$, according to Fig. 11, is roughly

$$(N_B - 1)\, D_x D_y \lesssim 2 \quad . \qquad (15)$$

This imposes a constraint on the allowable number of bunches per train.

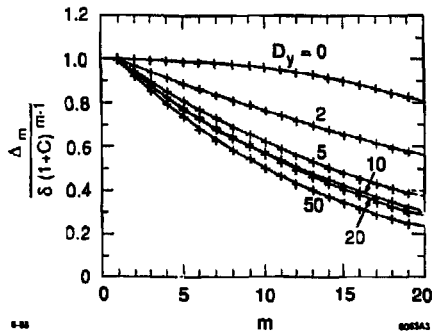

Fig. 11. Cumulative offset as a function of the number of bunches.

ENERGY SPECTRUM OF FINAL ELECTRONS

The energy spectrum of the electrons is important for two reasons: The *tip* of the spectrum, i.e., the distribution near the initial beam energy, provides information on the energy resolution for high energy physics events. On the other hand, the *tail* of the spectrum, i.e., the distribution of the low energy electrons, which had suffered severe energy loss through hard beamstrahlung, reveals the likelyhood of finding large disruption angles. This second issue will be addressed in the next section.

The energy spectrum of radiation can be characterized by the beamstrahlung parameter Υ, defined as

$$\Upsilon = \gamma \frac{B}{B_c} \quad , \qquad (16)$$

where B is the effective field strength of the beam, and $B_c = m^2c^3/e\hbar \sim 4.4 \times 10^{13}$ Gauss is the Schwinger critical field. For historical reasons, this parameter is related to the parameter ξ introduced by Sokolov and Ternov, by a simple factor

$$\xi = \frac{(\text{critical energy})}{(\text{initial energy})} = \frac{3}{2}\frac{r_e\gamma^2}{\alpha\rho} = \frac{3}{2}\Upsilon \quad , \qquad (17)$$

where ρ is the instantaneous radius of curvature. Since the two parameters are trivially related, we shall employ either of them depending on the convenience of the situation. The typical value of ξ during collision is

$$\xi_1 = \frac{r_e^2\gamma N}{\alpha\sigma_z\sigma_y}\frac{2}{1+R} \quad . \qquad (18)$$

The average value of ξ is a bit smaller than Eq. (18) (by about a factor 2/3) but we adopt Eq. (18) for the better description of the spectrum tail which is contributed more effectively from beamstrahlung with larger ξ.

The number of emitted photons per electron is

$$N_\gamma = N_{cl} U_0(\xi_1), \text{ with } N_{cl} = 2.12\frac{\alpha r_e N}{\sigma_z + \sigma_y} \quad , \qquad (19)$$

where N_{cl} is the number of photons computed by the classical formula and $U_0(\xi)$ is the ratio of the quantum-theoretical number of photons to that from the classical theory, and is found to be[6]

$$U_0(\xi) = \frac{1 - 0.598\xi + 1.061\xi^{5/3}}{1 + 0.922\xi^2} \quad , \qquad (20)$$

where the relative error is within 0.7%.

An approximate formula for the energy spectrum of electrons after collision has been derived recently. The details will be given in Ref. 10. Here we only quote the results. The distribution function $\psi(\varepsilon)$ ($\varepsilon = E/E_0$), normalized as $\int \psi(\varepsilon)d\varepsilon = 1$, can be written as

$$\psi(\varepsilon) \simeq e^{-N_\gamma}\left[\delta(\varepsilon - 1) + \frac{e^{-y}}{1-\varepsilon}h(N_1 y^{1/3})\right] \quad , \qquad (21)$$

with

$$h(x) = \frac{1}{2\pi i}\int_{\lambda-i\infty}^{\lambda+i\infty} \exp(xp^{-1/3} + p)dp \quad (\lambda > 0)$$
$$= \sum_{n=1}^{\infty} \frac{x^n}{n!\Gamma(n/3)} \qquad (22)$$

and

$$y = \frac{1}{\xi_1}(\frac{1}{\varepsilon} - 1) \quad ,$$

$$N_1 = \frac{1}{1+\xi_1 y} N_{el} + \frac{\xi_1 y}{1+\xi_1 y} N_\gamma \quad . \qquad (23)$$

(This formula does not exactly satisfy the normalization condition except for $\xi_1 \to 0$ which leads to $N_1 = N_\gamma = N_{el}$.) The function $h(x)$ can be estimated very accurately by with relative error less than 2%. Figure 12 compares Eq. (21) with the simulation results using the parameters for the TLC and the ILC.[11] The design parameters of the two colliders are summarized in Table 1. The histograms in Fig. 12 are from simulations and the dotted data are computed from Eq. (21). The agreement is excellent.

Table 1. Parameters for TLC and ILC ($\lambda_{rf} = 17mm$)

	TLC	ILC
E_0[TeV]	0.5	0.25
N	8×10^9	7×10^9
σ_x[nm]	190	440
σ_y[nm]	1	3
σ_z[μm]	26	65
R	190	147
ϵ_x [mrad]	2.58×10^{-12}	5.2×10^{-12}
ϵ_y [mrad]	2.33×10^{-14}	5.2×10^{-14}
D_x	0.033	0.027
D_y	6.27	3.9
A_x	0.0002	0.0017
A_y	0.60	0.37
* L/L_0	1.61	1.71
* δ	0.15	0.01
* N_γ	1.33	0.38
ζ_1	3.43	0.19

* Quantities computed by simulations.

MAXIMUM DEFLECTION ANGLE UNDER BEAMSTRAHLUNG

The particle which once lost a large fraction of its initial energy through beamstrahlung would in principle be severely deflected by the beam-beam field and cause background problems for high energy experiments. Consider an electron which emits a hard photon at a particular time during the collision and results in an energy εE_0,

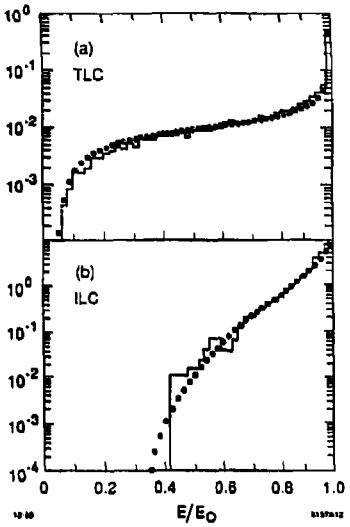

Fig. 12. Electron energy spectrum for TLC and ILC parameters.

with $\varepsilon \ll 1$. The effective disruption parameter for this particle becomes D_x/ε and D_y/ε. One might think that Eqs. (4) and (5) are still applicable by replacing D by D/ε. However, the collision of a single particle on a beam with the disruption parameter D/ε is different from the collision between two beams with D/ε, although the qualitative feature is the same; i.e., the disruption angle increases linearly in D for $D \lesssim 1$ and more slowly for $D \gtrsim 1$.

A simulation was done by monitoring low energy test particles through the collision process. The maximum deflection angle for a given ε is found to be roughly

$$\theta_{max} \sim \frac{\sigma}{\sigma_z} \frac{D/\varepsilon}{\sqrt{1+(0.75D/\varepsilon)^{4/3}}} \quad , \quad (\varepsilon \ll 1) \qquad (24)$$

where $D = D_x(D_y)$ and $\sigma = \sigma_x(\sigma_y)$ for the horizontal (vertical) angle.

The minimum value of ε can in principle be as small as $1/\gamma$. But the real problem is about how small a ε should one care. Since the number of photons N_γ per beam particle for linear colliders in the near future is of order unity, the spectral function $\psi(\varepsilon)$ given in Eq. (21) is always dominated by the factor e^{-y} in the spectrum tail, where $y \gg 1$ (in logarithmic sense). Therefore, if the acceptable background counts is n out of N electrons, then the minimum ε of concern is approximately determined by $y = \log(N/n)$, or

$$\varepsilon_{min} = \frac{1}{1+\xi_1 \log(N/n)} \quad . \qquad (25)$$

With this value of ε, one can directly estimate the maximum deflection angle using Eq. (24). Since the dependence

on n is only logarithmic, one can set $n = 1$. Thus, for example, $\epsilon_{min} = 0.013(0.188)$, $\theta_{x,max} = 10$ (0.95) mrad and $\theta_{y,max} = 0.4$ (0.15) mrad for TLC (ILC) parameters.

ADDENDUM: BEAMSTRAHLUNG PAIR CREATION

After the completion of this paper, the author identified a new phenomenon called "coherent beamstrahlung pair creation",[12] which, together with the incoherent process studied earlier,[13,14] would have impacts on linear collider designs. Recall that in the case of radiation by $e^-(e^+)$ during beam-beam collision, there are essentially two mechanisms that induce the radiation. Namely, there is an "incoherent" process, or Bremsstrahlung, associated with the individual e^-e^+ scatterings, and there is also a "coherent" process due to the interaction between the radiating charged particle and the macroscopic beam-beam EM field. At high energies and strong fields, the coherent process tends to dominate over the incoherent one. This is actually why our discussion on beam energy loss has been focused only on the beamstrahlung process.

The beamstrahlung photons once emmited would have to travel through the remainder of the oncoming beam before entering into free space, and would therefore turn themselves into e^-e^+ pairs. Analogous to the case of radiation, photon pair creation also involves coherent and incoherent processes. Here again, at high energies and strong fields the coherent process will dominate over the incoherent one. Once the e^-e^+ pairs are created with lower energies in general, one of the two particles in each pair will have the same sign of charge as the oncoming beam (For the sake of argument, consider a low energy e^+ moving against the positron beam). Unlike the case of low energy e^- moving against a positron beam, where the potential tends to confine the particle in the beam profile, in the case of a positron the potential is unconfining, and the particle can in principle be deflected by a large angle and thus create severe background problems. This effect would therefore impose a contraint on the final focus design.

It is well known that the cross section for incoherent pair creation is

$$\sigma(\gamma e \to e e^+ e^-) \sim \frac{28}{9}\alpha r_e^2 \log\Big(\frac{2\omega E}{m^2}\Big)\mathrm{cm}^2 \quad , \qquad (26)$$

which is a very slowly varying function of the photon energy ω. For TLC, $\gamma = 1 \times 10^6$, the cross section is $\sim 5\times10^{-26}$ cm^2 for photons at full energy. The beam parameters for TLC listed in the above Table gives the average number of the beamstrahlung photon per beam particle as $N_\gamma \sim 1.3$. On the other hand, it can be shown[13] that the effective luminosity for such a cascading process is 1/2 of the original. Thus, the number of e^-e^+ pairs created per bunch crossing can be easily evaluated to be

$$N^1_{e^+e^-} = \frac{1}{2}\sigma(\gamma e \to e e^+ e^-)\frac{N_\gamma L_{ee}}{f_{rep}} \sim 2\times10^5 \quad , \qquad (27)$$

where $L_{ee} = 1.3 \times 10^{33}\mathrm{cm}^{-2}\mathrm{sec}^{-1}$, and $f_{rep} = 220\ \mathrm{sec}^{-1}$ in this design. To be sure, this process provides a non-negligible amount of e^-e^+ pairs.

The rate of photon pair creation in a homogeneous magnetic field has been studied by many people[15] and has been generalized to inhomogeneous fields by Baier and Katkov.[16] In the asymptotic limits the rate can be expressed as

$$\frac{dI}{dt} = \begin{cases} \frac{2\sqrt{3}}{16\sqrt{2}}\frac{\alpha\Upsilon}{\lambda_c\gamma}e^{-8/3\chi} & , \ \chi \ll 1 \ ; \\ \frac{15}{4}\left(\frac{3}{2}\right)^{1/3}\frac{\Gamma(5/6)}{\Gamma(1/6)}\frac{\alpha\Upsilon}{\lambda_c\gamma}\chi^{-1/3}\Big] & , \ \chi \gg 1 \ . \end{cases} \qquad (28)$$

Here $\chi = \Upsilon\omega/E$ plays the similar role as Υ in the case of beamstrahlung. Notice that χ is independent of the initial particle energy γ, as the process does not care where the photon was originated from. Let

$$\frac{dI}{dt} \equiv \frac{\alpha\Upsilon}{\lambda_c\gamma}T(\chi) \quad . \qquad (29)$$

To a very good approximation,[17]

$$T(\chi) = 0.16\chi^{-1}K^2_{1/3}\Big(\frac{4}{3\chi}\Big) \quad . \qquad (30)$$

for all values of χ.

Integrating over the collision time — again, only half of the e^-e^+ collision time — we have

$$\begin{aligned} I &= \frac{\sqrt{3}}{2}\frac{\sigma_z\alpha\Upsilon}{\lambda_c\gamma}T(\chi) \\ &= \frac{1}{2}n_{el}T(\chi) \quad . \end{aligned} \qquad (31)$$

Next we evaluate the mean value of $T(\chi)$ by weighting over the beamstrahlung spectral function,

$$\frac{dn_\delta}{d\omega} = \frac{1}{\pi}\frac{\alpha\sigma_z}{\gamma^2}\left\{\int_y^\infty K_{5/3}(x)dx + \frac{\xi^2y^2}{1+\xi y}K_{2/3}(y)\right\} \quad . \qquad (32)$$

and

$$\langle T(\Upsilon)\rangle = \int_0^E T(\chi)\frac{dn_\delta}{d\omega}d\omega \Big/ \int_0^E \frac{dn_\delta}{d\omega}d\omega \quad . \qquad (33)$$

The total number of e^-e^+ pairs created through this coherent process is therefore

$$N^c_{e^+e^-} = \frac{1}{2}N_\gamma n_{el}\langle T(\Upsilon)\rangle \quad . \qquad (34)$$

A plot of $\langle T(\Upsilon)\rangle$ is shown in Fig. 13, where the solid curve is from the exact form of $dn_\delta/d\omega$ in Eq. (32), and the dashed curve corresponds to an asymptotic expression for $dn_\delta/d\omega$ at large y. The closeness between the two curves

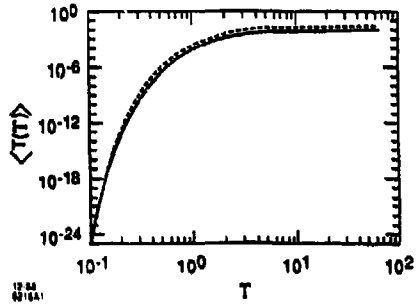

Fig. 13. The function $\langle T(\Upsilon) \rangle$ vs. Υ.

suggests that only the spectrum tip contribute effectively to the coherent pair creation process. From the TLC parameters, $n_{cl} \sim 1.9$, so we find that

$$N^c_{e^+e^-} \sim 5 \times 10^7 \quad , \qquad (35)$$

which is much larger than the incoherent process.

It should be noticed, however, that $\langle T \rangle$ drops exponentially for $\Upsilon \lesssim 1$. Therefore, for next generation linear colliders at the range of 1 TeV, which would typically have $\Upsilon \sim 1$, it is not at all difficult to redesign the machine such that the coherent process can be entirely suppressed. For the above-mentioned TLC parameters the condition is $\Upsilon \lesssim 0.3$. This, ironically, is an over-kill of the issue since the incoherent process corresponds to $\Upsilon \sim 0.6$, as can be read from Fig. 13.

Since to a large extent N_γ is of the order unity and quite insensitive to other parameters, and since we usually choose to fix the luminosity in a design, the incoherent e^-e^+ pairs can not be easily suppressed. It is thus important to evaluate the energy spectrum of the pair created e^+. Assuming constant probability in finding the e^+ at energy $\varepsilon E \leq \omega$, the spectrum can be derived to be

$$N_{e^+}(\varepsilon) = \frac{7(3/2)^{2/3}}{18\pi^2\Gamma(1/3)} \frac{\alpha^3}{\gamma m} N D_y \Upsilon^{2/3} F(\varepsilon, \Upsilon) \quad . \qquad (36)$$

The spectral function $F(\varepsilon, \Upsilon)$ is plotted in Fig. 14 for $\Upsilon = 0.2$. At the small ε limit, $F(\varepsilon, \Upsilon) \propto 1/\varepsilon$.

Finally, we evaluate the deflection angle of these low energy positrons by the beam-beam field. As a rough estimation, we assume that the vertical field beyond the beam height extents constantly to a distance equal to the beam width σ_x. It can be shown[10] that the deflection angle for the e^+ with energy ε is

$$\theta_\varepsilon = \begin{cases} \frac{2}{3\Gamma(\frac{1}{3})} \frac{\sigma_z}{\sigma_x} \sqrt{\frac{D_x}{\varepsilon}} \quad , & \theta_\varepsilon \geq \frac{2}{\sqrt{3}} \theta_d \quad ; \\ 2 \frac{\sigma_z}{\sigma_x} \frac{D_x}{\varepsilon} \quad , & \theta_\varepsilon \leq \frac{2}{\sqrt{3}} \theta_d \quad . \end{cases} \qquad (37)$$

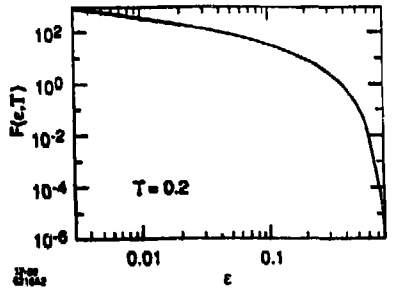

Fig. 14. The spectral function for incoherent pair created e^+.

The deflection angle in the above expression is plotted in Fig. 15. For a 1 GeV e^+, $\theta_\varepsilon \sim 45$ mrad. The information on the transverse momentum can be easily deduced from the above expressions via $p_\perp = \varepsilon\theta_\varepsilon$.

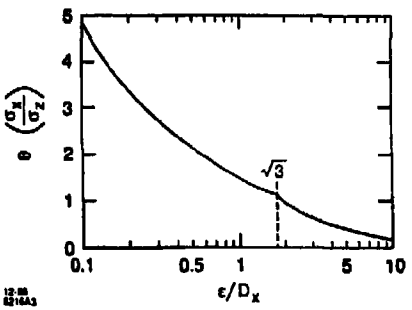

Fig. 15. The deflection angle as a function of e^+ energy.

REFERENCES

1. K. Yokoya, *A Computer Simulation Code for the Beam-Beam Interaction in Linear Colliders*, KEK Report 85-9, Oct 1985.
2. P. Chen and K. Yokoya, *Disruption Effects from the Interaction of Round e^+e^- Beams*, Phys. Rev. D **38**, 987 (1988).
3. P. Chen and K. Yokoya, *Disruption Effects from the Interaction of flat e^+e^- Beams*, in preparation.
4. W. M. Fawley and E. P. Lee, *Particle in Cell Simulations of Disruption*, in "New Developments in Particle Acceleration Techniques", Orsay 1987, CERN 87-11, ECFA 87/110.
5. R. Holebeek, *Disruption Limits for Linear Colliders*, Nucl. Ins. Meth. 184 (1981).

6. N. A. Solyak, *Collision Effects in Compensated Bunches of Linear Colliders*, Novosibirsk Preprint IYF-88-44, 1988.

7. K. Yokoya and P. Chen, *Multiple Bunch Crossing Instability*, SLAC-PUB-4653, June 1988.

8. Y. H. Chin, *Stability of a Colliding Beam in a Linear Collider*, DESY January 1987.

9. K. Yokoya and P. Chen, *Depolarization due to Beam-Beam Interaction in Electron-Positron Linear Colliders*, SLAC-PUB-4692, September 1988; and in the *Proceedings for the Eighth International Symposium on High Energy Spin Physics*, 1988.

10. P. Chen and K. Yokoya, *Final Electron Energy Spectrum and Maximum Deflection Angle under Beamstrahlung*, in preparation.

11. R. B. Palmer, *Interdependence of Parameters for TeV Linear Colliders*, SLAC-PUB-4295, April 1987; and SLAC-AAS-39, November 1988.

12. P. Chen, *Review of Beam-Beam Interaction*, summary talk given at the International Workshop on the Next Generation Linear Colliders, November 28-December 9, 1988, SLAC, Stanford.

13. M. S. Zolotarev, E. A. Kuraev and V. G. Serbo, *Estimates of Electromagnetic Background Processes for the VLEPP Project*, Inst. Yadernoi Fiziki, Preprint 81-63, 1981; English translation SLAC TRANS-0227, 1987.

14. I. F. Ginzburg, G. L. Kotkin, V. G. Serbo and V. I. Telnov, *Colliding γe and $\gamma\gamma$ Beams Based on the Single-Pass Accelerators*, Inst. Nucl. Phys. (Novosibirsk) Preprint 81-102, 1981.

15. See, for example, W. Y. Tsai and T. Erber, Phys. Rev. D **10**, 492, 1974; and references therein.

16. V. N. Baier and V. M. Katkov, Soviet Phys. JETP **26**, 854, 1968.

17. T. Erber, Rev. Mod. Phys. **38**, 626, 1966.

18. V. I. Telnov, private communications.

DISCLAIMER